CHIN. PHYS. LETT. Vol. 37, No. 12 (2020) 127101

HfX_2 (X = Cl, Br, I) Monolayer and Type Ⅱ Heterostructures with Promising Photovoltaic Characteristics

Xingyong Huang(黄兴勇)[1,2,3], Liujiang Zhou(周柳江)[3*], Luo Yan(燕罗)[3], You Wang(王渊)[1], Wei Zhang(张伟)[1], Xiumin Xie(谢修敏)[1], Qiang Xu(徐强)[1], and Hai-Zhi Song(宋海智)[1,3*]

[1]*Southwest Institute of Technical Physics, Chengdu 610041, China*
[2]*Faculty of Science, Yibin University, Yibin 644007, China*
[3]*Institute of Fundamental and Frontier Sciences, University of Electronic Science and Technology of China, Chengdu 610054, China*

(Received 10 September 2020; accepted 26 October 2020; published online 8 December 2020)

Two-dimensional (2D) materials and their corresponding van der Waals (vdW) heterostructures are considered as promising candidates for highly efficient solar cell applications. A series of 2D HfX_2 (X = Cl, Br, I) monolayers are proposed, via first-principle calculations. The vibrational phonon spectra and molecular dynamics simulation results indicate that HfX_2 monolayers possess dynamical and thermodynamical stability. Moreover, their electronic structure shows that their Heyd–Scuseria–Ernzerhof(HSE06)-based band values (1.033–1.475 eV) are suitable as donor systems for excitonic solar cells (XSCs). The material's significant visible-light absorbing capability ($\sim 10^5\,\mathrm{cm}^{-1}$) and superior power conversion efficiency (∼20%) are demonstrated by establishing a reasonable type Ⅱ vdW heterostructure. This suggests the significant potential of HfX_2 monolayers as a candidate material for XSCs.

PACS: 71.15.Mb, 71.20.−b, 88.40.H− DOI: 10.1088/0256-307X/37/12/127101

Solar cells, which convert solar energy into electricity, are an environmentally friendly energy conversion device, contributing to sustainable development in terms of global technology.[1] Employed in conventional commercial photovoltaic devices, silicon-based solar cells have a theoretical limit, in terms of energy conversion efficiency, of 29.1%.[2] In the search to improve upon this level of efficiency, the investigation of alternative energy materials to replace silicon has become a hot topic. With this aim in view, two-dimensional (2D) type Ⅱ vdW heterostructures, with their extraordinary electronic, optical, and mechanical properties,[3,4] and specifically the ultra-high specific surface area of a monolayer, with its effective electron-hole separation, are anticipated to replace silicon-based solar cells in the next generation of high-efficiency solar cells. Although 2D type Ⅱ vdW heterostructures have been designed for photovoltaic devices, their energy conversion efficiency is as yet unsatisfactory.[5]

In this regard, the 2D ⅣB–ⅦA-group transition-metal halides (ⅣGTMHs), a new family of 2D semiconductors, have exhibited many novel properties, such as the quantum spin Hall effect, and large nontrivial band gaps.[6] In this work, we focus on a heterojunction composed of HfX_2 (X = Cl, Br, I) monolayers, a material belonging to the 2D ⅣGTMH group, which serves as a kind of layered compound for photovoltaic applications. Based on first-principles calculations, we evaluate the stability of HfX_2 monolayers, predict 2D type Ⅱ vdW heterostructures, and calculate their power conversion efficiency (PCE) for excitonic solar cells (XSCs).

The Vienna *ab initio* simulation package (VASP) is used to implement our density functional theory (DFT) calculations.[7,8] The frozen-core projector-augmented wave (PAW) method[7,8] is also applied. The Perdew–Burke–Ernzerhof (PBE) function within the generalized gradient approximation (GGA)[9] is used to describe the exchange-correlation interaction of electrons. To take into account the vdW interaction between different monolayers in the heterostructures, the OptB88vdW method[10] is adopted. With regard to calculations for monolayers, inter-monolayer interactions are considered negligible, given that the vacuum thickness is set to more than 15 Å from the border in the Z direction. The energy cut-off for the planewave basis is set at 420 eV. The convergence criteria of total energy and force are 10^{-6} eV and 0.001 eV/Å, respectively. The canonical ensemble, with a Nose–Hoover thermostat[11] at 300 K for 10 ps, is performed via molecular dynamics simulations, so as to evaluate thermodynamic stability. The Phonopy code[12] is used to calculate phonon dispersion, in order to assess the material's dynamical stability. More accurate band edge characteristics are

Supported by the National Key Research and Development Program of China (Grant No. 2017YFB0405302).
*Corresponding authors. Email: liujiang86@gmail.com; hzsong1296@163.com;
© 2020 Chinese Physical Society and IOP Publishing Ltd

obtained using Heyd–Scuseria–Ernzerhof (HSE06) hybrid functions.[13]

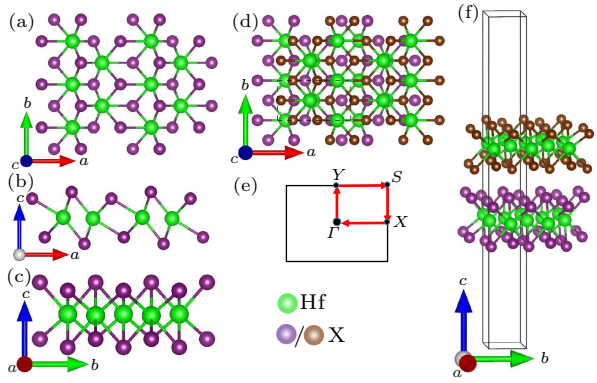

Fig. 1. Top (a) and side [(b), (c)] view of the crystal structure of the HfX_2 monolayer, together with the top (d) and side (f) view of the crystal structure of the designed 2D vdW heterostructures. (e) First Brillouin zone of HfX_2 monolayers, with their points of high symmetry.

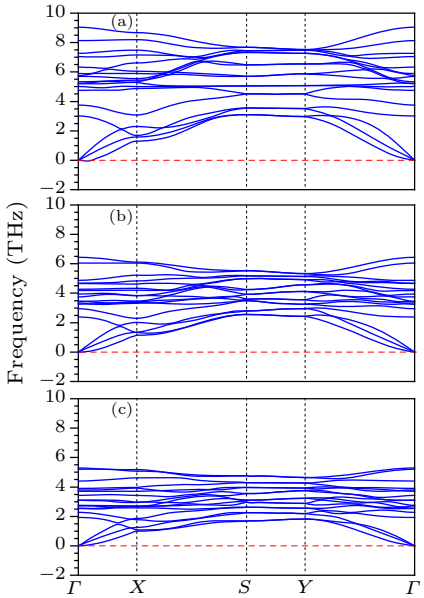

Fig. 2. Phonon spectra of (a) $HfCl_2$, (b) $HfBr_2$, and (c) HfI_2. Γ, X, S, and Y correspond to the (0.0, 0.0, 0.0), (0.5, 0.0, 0.0), (0.5, 0.5, 0.0), and (0.0, 0.5, 0.0) k-points in the first Brillouin zone, respectively.

Figures 1(a)–1(c) and 1(d) depict the crystal structures of the HfX_2 monolayer, and the design of the vdW heterojunctions. The HfX_2 monolayer hosts a rectangular lattice, where the Hf is enclosed in an HfX_6 octahedron. The HfX_2 monolayer possesses a 1T'-MoS_2 structure, such that the Hf is not positioned centrally in the HfX_6 octahedron. Figure 1(e) shows the corresponding high symmetry points in the first Brillouin zone. The 2D structure in Figs. 1(d) and 1(f) is a vertical vdW heterostructure, and with the upper and lower layers being composed of different HfX_2 monolayers. The lattice parameters of the fully optimized HfX_2 monolayer are shown as follows: $a = 6.144$ and $b = 3.2686.144$ Å for $HfCl_2$; $a = 6.416$ and $b = 3.429$ Å for $HfBr_2$; $a = 6.814$ and $b = 3.707$ Å for HfI_2. Note that a larger atomic radius corresponds to a larger lattice parameter.

Vibrational phonon spectra are employed to assess dynamical stability. Having been fully optimized, the phonon spectra of the HfX_2 monolayers along the high-symmetry points are then calculated (see Fig. 2). The absence of imaginary frequencies in the phonon spectra indicates that HfX_2 monolayers are dynamically stable. The highest frequency of the HfX_2 monolayer phonon spectrum is ~10 THz (~350 cm^{-1}), which is comparable to MoS_2 (~350 cm^{-1})[14] and smaller than silicene (~580 cm^{-1}),[15] suggesting that the bond strength of Hf–X is lower than that of Si–Si. In order to further evaluate the stability of the HfX_2 monolayer, the thermodynamic stability (molecular dynamic) criterion was adopted. The results of a molecular dynamics simulation at 300 K (see Fig. 3) depict the total energy and fluctuations as a function of simulation time. Ignoring thermal fluctuations, it is evident that the HfX_2 monolayer shows no obvious structural deterioration after 10 ps, indicating that the HfX_2 monolayer is thermally stable at room temperature.

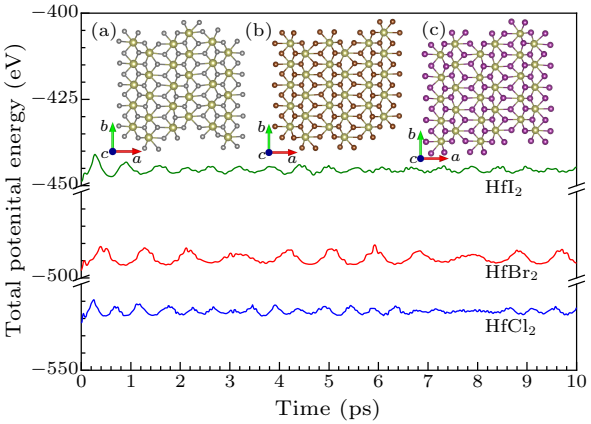

Fig. 3. Evolution of potential energy with respect to simulation time at 300 K for the HfX_2 monolayer. Final snapshots for $HfCl_2$, $HfBr_2$ and HfI_2 are shown in (a), (b) and (c), respectively.

The HSE06-based electronic structural properties of the HfX_2 monolayer are shown in Figs. 4(a)–4(c). The bandgap values of $HfCl_2$, $HfBr_2$, and HfI_2 are 1.475, 1.337, and 1.033 eV, respectively. Evidently, halogens with larger atomic sizes would reduce the bandgap. This is understandable, given that the increment of the bond lengths of the HfX_2 (Cl → Br → I) monolayer reduces the repulsive effect, similarly to the behavior of bulk semiconductors.[16] In particular, the valence and conduction bands are primarily contributed by Hf atoms. The Hf-d (xy, x^2–y^2) orbit dominates the conduction band minimum (CBM) and valence band maximum (VBM), and halogens primarily affect the deep energy levels. Figures 5(a)–5(c)

illustrate the band structure of the heterojunction, depicting the valence and conduction band edges referenced to vacuum level, and indicating three possible designs for type Ⅱ vdW heterojunction structures ($HfI_2/HfCl_2$, $HfI_2/HfBr_2$, and $HfBr_2/HfCl_2$). The square of dipole moment transition matrix elements was calculated to evaluate the electronic transition between valence and conduction bands. As shown in Figs. 4(d)–4(f), the dominant transition probability is concentrated to the in-plane states of the Hf atoms, where the maximum transition probability occurs in the 2nd to 3rd band for region I, and the 1st to 3rd band for region Ⅱ. Moreover, the halogens enable the tuning of the transition probability competitiveness of regions I and Ⅱ.

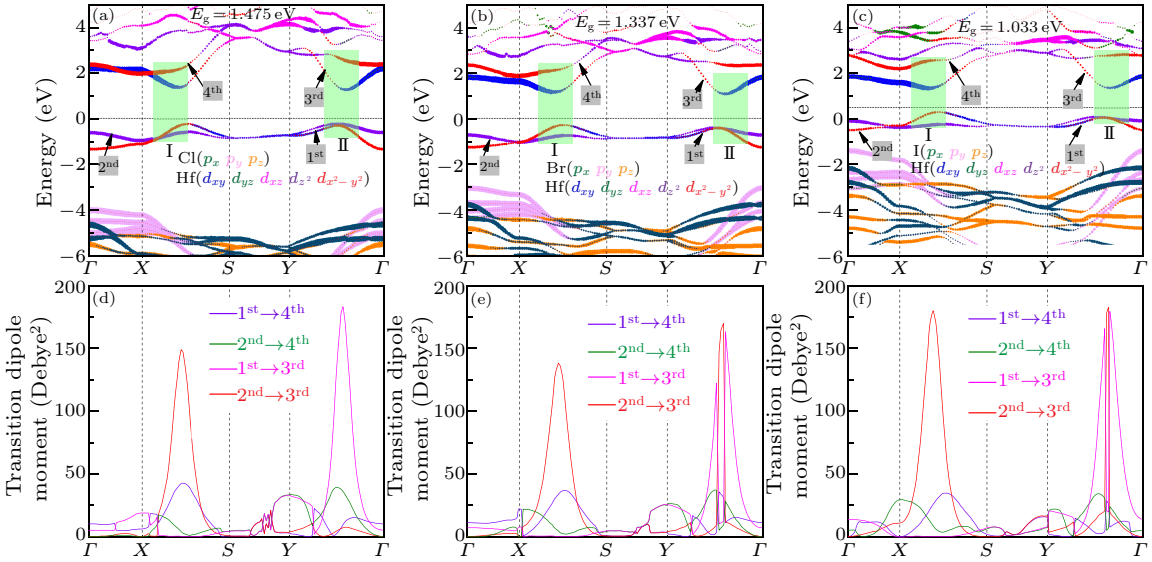

Fig. 4. HSE06-based band structure, with the corresponding transition dipole moment for [(a), (d)] $HfCl_2$, [(b), (e)] $HfBr_2$, and [(c), (f)] HfI_2 monolayers. Regions I and Ⅱ, corresponding to the pale green shaded areas, are utilized to mark the main dipole moment transition process. The 2nd band is the highest occupied valence band. The Fermi level is set to zero.

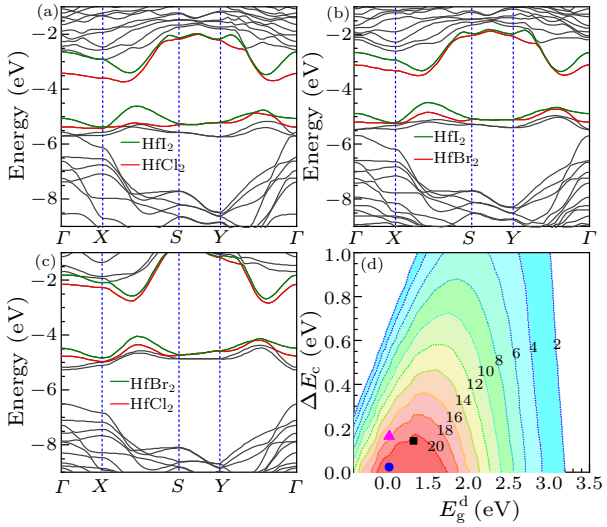

Fig. 5. Band structure of $HfI_2/HfCl_2$ (a), $HfI_2/HfBr_2$ (b), and $HfBr_2/HfCl_2$ (c) heterostructures. The solid lines in red and green represent the highest occupied and the lowest non-occupied state of $HfCl_2$ ($HfBr_2$ and HfI_2). (d) PCE contour as a function of E_g^d and ΔE_c. The PCE limits of $HfI_2/HfCl_2$, $HfI_2/HfBr_2$, and $HfBr_2/HfCl_2$ heterostructures are indicated by a pink triangle, a blue circle, and a black square, respectively.

Clearly, vdW (vertical) heterostructures can be applied effectively to XSCs.[17–19] Here, the adopted vdW (vertical) heterostructure configuration has been optimized by searching for that with the lowest energy, which is the most stable stacking method. For the type Ⅱ vdW heterojunction XSCs, the PCE was calculated following Scharber's method.[20] The upper limit of PCE can be calculated in the limit of 100% external quantum efficiency, which can be expressed as[20]

$$\eta = \frac{0.65(E_g^d - \Delta E_c - 0.3)\int_{E_g^d}^{\infty} \frac{P(\hbar\omega)}{\hbar\omega} d(\hbar\omega)}{\int_{E_g^d}^{\infty} P(\hbar\omega) d(\hbar\omega)},$$

where 0.65 is a band-filling factor deduced from the Shockley–Queisser limit, and $P(\hbar\omega)$ denotes the AM1.5 solar energy flux at the photon energy, $\hbar\omega$. The parameter 0.3 eV is used to explain the energy conversion kinetics. Including the band gap of the donor (E_g^d), and the conduction band offset (ΔE_c), taken from the HSE06 calculations. Figure 5(d) shows the PCE contour plots for all type-Ⅱ heterostructures. Clearly, small ΔE_c and suitable E_g^d (∼1.3 eV) would result in satisfactory PCEs. The PCEs for $HfI_2/HfCl_2$, $HfI_2/HfBr_2$, and $HfBr_2/HfCl_2$ are 17.150%, 21.438%, and 20.439%, respectively. These values are comparable with the PCE of polycrystalline CdTe thin films (21.5%)[20,21] and per-

ovskite (22.1%)[20,22] solar cells, and higher than dye-sensitive (∼12%)[20,21] and organic (∼12%)[20,23,24] solar cells. Moreover, the efficiency of XSCs is dependent on their sunlight absorption capacity. The HSE06-calculated optical absorption spectra are given in Fig. 6, with the incident AM1.5 G solar spectrum shown for comparison. The results reflect an excellent sunlight absorption performance, as compared with that previously reported for intrinsic silicon.[25] Since the HfX_2 monolayer is anisotropic, all heterojunctions appear to absorb near-ultraviolet light in the x direction, and visible light in the y direction. In addition, the heterojunction structure results in a peak characteristic at ∼900 nm [Fig. 6(b)] and the harvesting of visible light in the y direction. The visible light harvesting capacity of the heterojunctions reaches as much as $10^5\,\mathrm{cm}^{-1}$ in the y direction, which is comparable to, or even higher than, intrinsic silicon and organic perovskite materials (10^4–$10^5\,\mathrm{cm}^{-1}$),[26] and is higher than the absorption coefficient reported for other 2D materials in visible light, such as phosphaalkene[27] and $MnPSe_3$ monolayers.[28] The optical absorption spectra suggest that the heterostructures considered here can efficiently utilize solar energy.

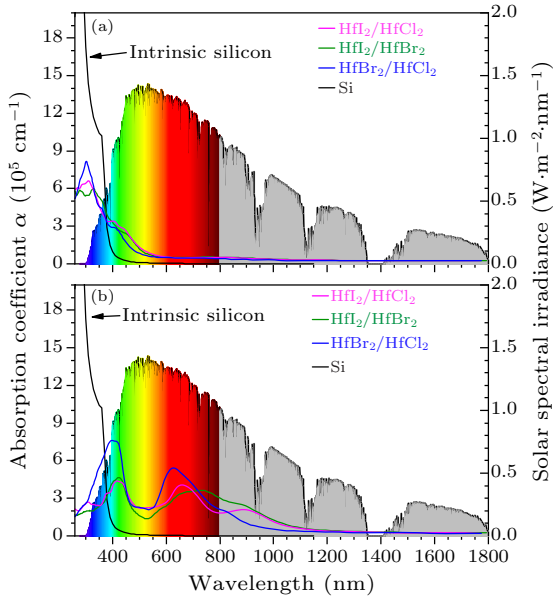

Fig. 6. Optical absorption spectra in the x (a) and y (b) directions, calculated via the HSE06 method. The colored region indicates the visible light spectrum.

In summary, we have investigated the geometry, stability, and electronic structures of the HfX_2 monolayer, and related type Ⅱ vdW heterostructures. The results suggest that the HfX_2 monolayer is dynamically and thermodynamically stable. A PCE of over 20% corresponds to E_g^d between ∼0.9 and ∼1.7 eV, suggesting bandgap values (1.033–1.475 eV) favorable to the donor system as XSCs. Furthermore, the valence band and conduction band around the Fermi level are primarily determined by the Hf-d orbit. More importantly, significant visible light absorbing capability (∼$10^5\,\mathrm{cm}^{-1}$) and impressive PCE (17.150%, 21.438% and 20.439%) can be obtained by establishing type Ⅱ vdW heterostructures for XSCs, demonstrating great potential for future solar energy conversion applications.

The authors wish to thank Qiang Zhou, Guangwei Deng and Lei Hu for useful discussions.

References

[1] Yue G, Deng Z, Wang S *et al.* 2019 *Chin. Phys. Lett.* **36** 057201
[2] Essig S, Allebé C, Remo T *et al.* 2017 *Nat. Energy* **2** 17144
[3] Cheng K, Guo Y, Han N *et al.* 2018 *Appl. Phys. Lett.* **112** 143902
[4] Fang J, Zhou Z, Xiao M *et al.* 2020 *InfoMat* **2** 291
[5] Pospischil A, Furchi M M and Mueller T 2014 *Nat. Nanotechnol.* **9** 257
[6] Zhou L, Kou L, Sun Y *et al.* 2015 *Nano Lett.* **15** 7867
[7] Kresse G and Furthmüller J 1996 *Comput. Mater. Sci.* **6** 15
[8] Kresse G and Furthmüller J 1996 *Phys. Rev. B* **54** 11169
[9] Perdew J P, Burke K and Ernzerhof M 1996 *Phys. Rev. Lett.* **77** 3865
[10] Klimeš J, Bowler D R and Michaelides A 2010 *J. Phys.: Condens. Matter* **22** 022201
[11] Nosé S 1984 *J. Chem. Phys.* **81** 511
[12] Mann S, Rani P, Kumar R *et al.* 2015 *AIP Conf. Proc.* **1675** 030035
[13] Krukau A V, Vydrov O A, Izmaylov A F *et al.* 2006 *J. Chem. Phys.* **125** 224106
[14] Molina-Sánchez A and Wirtz L 2011 *Phys. Rev. B* **84** 155413
[15] Cahangirov S, Topsakal M, Aktürk E *et al.* 2009 *Phys. Rev. Lett.* **102** 236804
[16] Lü T Y, Liao X X, Wang H Q *et al.* 2012 *J. Mater. Chem.* **22** 10062
[17] Lai K, Yan C L, Gao L Q *et al.* 2018 *J. Phys. Chem. C* **122** 7656
[18] Zhou L J, Zhang Y F and Wu L M 2013 *Nano Lett.* **13** 5431
[19] Kaur S, Kumar A, Srivastava S *et al.* 2018 *J. Phys. Chem. C* **122** 26032
[20] Scharber M C, Mühlbacher D, Koppe M *et al.* 2006 *Adv. Mater.* **18** 789
[21] Green M A, Emery K, Hishikawa Y *et al.* 2015 *Prog. Photovoltaics* **23** 1
[22] Green M A, Emery K, Hishikawa Y *et al.* 2017 *Prog. Photovoltaics* **25** 3
[23] Zhao J, Li Y, Yang G *et al.* 2016 *Nat. Energy* **1** 15027
[24] Dai J and Zeng X C 2014 *J. Phys. Chem. Lett.* **5** 1289
[25] Miao N, Xu B, Bristowe N C *et al.* 2017 *J. Am. Chem. Soc.* **139** 11125
[26] Lu X, Zhao Z, Li K *et al.* 2016 *RSC Adv.* **6** 86976
[27] Jiao N, Zhou P, Xue L *et al.* 2019 *J. Phys.: Condens. Matter* **31** 075702
[28] Zhang X, Zhao X, Wu D *et al.* 2016 *Adv. Sci.* **3** 1600062